# Retrieval of Temperature and Humidity from GPS-Radio Occultation derived Refractivity using Physical Iterative Method: Operational Algorithm for MT-ROSA

**Abhineet Shyam**[*]

## Abstract

This paper discusses the retrieval algorithm based on physical iterative method that demarcates the atmosphere into the dry and moisture-containing region at the threshold height, which is dynamically parameterized in terms of temperature that is verified through a sensitivity study. The algorithm retrieves the temperature and pressure for the entire atmosphere after neglecting the water vapour term in the refractivity forward model. The geophysical profiles are, to a very good approximation, true to the actual profile of temperature and pressure beyond the threshold height. Below this height, the true temperature varies quadratically with natural logarithm of pressure and is the basis of retrieval for the moisture-containing region.

The algorithm is applied on refractivity forward modeled from NCEP analyses data and the retrieved geophysical parameters (GPs) are compared against NCEP. The temperature and water vapour partial pressure are largely within 1 K and less than 0.6 mb, respectively. The algorithm is subsequently applied on satellite-derived refractivity from COSMIC mission and the retrieved GPs are compared to collocated radiosonde with standard deviation within 2 K between 5 – 30 km for temperature and better than 2 mb between 5 – 16 km for the water vapour partial pressure. Differences between tropics and global statistics are seen below 5 km in both the parameters.

**Keywords:** Retrieval, GPS-RO, Refractivity, COSMIC, Temperature, Humidity.

---

Geophysical parameter Retrievals Division, Atmospheric and Oceanic Sciences Group (AOSG), EPSA, Space Applications Centre (SAC), ISRO, Ahmedabad.

[*] *Mr. Abhineet Shyam*
*Room No. 6047, Space Applications Centre, ISRO,*
*Bopal Campus, Bopal, Ahmedabad-380058*
*e-mail: abhineetshyam@sac.isro.gov.in*

## 1. INTRODUCTION

GPS-radio occultation sounding of the Earth's atmosphere, beginning with GPS-MET experiment in 1996 [1], has shown its worth for weather and climate studies with each successive mission viz. Oersted [2], SUNSAT [3], CHAMP [4], SAC-C [5], GRACE [6], COSMIC/FORMOSAT-3 [7], GRAS/METOP Series [8], Oceansat-2/ROSA [9], Megha-Tropiques (MT)-ROSA and recently, TerraSAR-X [10] and GNOS/FY3-C [11]. The strengths of this limb sounding technique includes all-weather measurement with high climate quality stability, exceptionally high vertical resolution and low power-low cost requirements in terms of hardware realization and longer mission life. These unique qualities of GPS-RO have been harnessed for use as a calibration and verification standard for radiometer, primarily, because of its distinct physical principles which provide independent comparison [12]. Due to its capability to provide sounding data over oceans as well, make it a reliable substitute for radiosonde observations which are hardly available over the vast oceans and seas of the Earth. It also has an unprecedented capability of providing absolute geopotential heights of its measurements with an accuracy of 10 m [13]. The impact of GPS-RO data has been strongly felt in improvement of the skills of weather forecast models. Owing to these varied and critical advantages, the GPS-RO technique has received greater attention in recent years and the need for more of such missions have been spelt out for future times to come [14].

In this paper, we have developed an algorithm for retrieval of geophysical parameters from radio occultation refractivity and demonstrate its performance by applying it firstly on refractivity simulated from NCEP analyzed fields. Subsequently, the algorithm is applied on operational refractivity products from COSMIC radio occultation mission and is compared with collocated radiosonde fields. Operational geophysical products from COSMIC 1DVAR method are compared statistically to collocated radiosonde fields to evaluate the performance of the developed algorithm.

The basic observables of GPS-RO technique are phase and amplitude of the dual-frequency signals from GPS satellites, recorded by the GPS receiver in a limb sounding geometry. The excess phase, due to the atmospheric delay of the signals causing the ray path to bend from its straight line path, is differentiated with respect to time to derive excess Doppler. This, in turn, is related to bending angle of the ray signal as a function of the impact parameter. The inversion of bending angle to refractivity is carried out using the Abel integral transform [15] under the local spherical symmetry assumption of the Earth's atmosphere. The refractivity, so derived, is inverted to retrieve temperature, pressure and water vapor partial pressure for the neutral atmosphere (below 60 km). A detailed technical description of the radio occultation technique including the procedure for inversion of raw signal to refractivity is given in [16]. Two popular techniques for retrieval of atmospheric profiles from refractivity have been the one-dimensional variational method (1DVAR) [17], [18], [19], [20] based on statistical optimization approach and the physical/empirical iterative method [16], [21], [22], [23]. Section 2 gives a detailed description of the physical iterative retrieval methodology for inversion of GPS-RO refractivity to geophysical parameters. Section 3 deals with results of retrieval from

refractivity by assuming water-vapour free atmosphere and demonstrating the seasonal and geographical characteristics of the validation results. In section 4, firstly, the results of retrieval from simulated refractivity from NCEP analyses data are shown, and secondly, the performance of the algorithm over COSMIC refractivity data is described with respect to radiosonde data as a reference dataset. Additionally, for an assessment of the performance of the algorithm vis-a'-vis COSMIC 1DVAR algorithm, COSMIC operational geophysical products are validated against the collocated radiosonde data. The concluding remarks are presented in section 5.

## 2. RETRIEVAL METHODOLOGY

The retrieval algorithm is a two-tier approach based on a demarcation of the Earth's atmosphere into a moisture-free ("dry") and a moisture-containing ("wet") part. Such a demarcation follows empirically from the observation of a dominant presence of water vapor in the lower-mid troposphere, generally up to 12-14 km in the tropics and 6-8 km in the extra-tropics. The atmosphere above is either completely dry or has minor traces of water vapor, which can be neglected. The "wet" refractivity term arises from the large permanent dipole moment of water vapor and becomes significant in the lower troposphere. With more moisture loading towards the lower part of the "wet" atmosphere, higher value of refractive index is observed moving down the atmosphere. Further, there is a large variation in the spatio-temporal concentration of water vapor in the "wet" atmosphere, especially in the tropics than in the mid-latitude and Polar region. Thus, the dominance of water vapor in the tropical "wet" atmosphere, coupled with its dynamical nature, causes the refractive index, and in turn, the refractivity to show large variation about the mean trend. The dynamical range of refractivity is quite narrow in the sub-tropical mid latitude and Polar region.

It is now seen to be meaningful and mathematically plausible to separate out the effect of water vapor on the refractivity in the "dry" atmosphere by considering only the dry part of the refractivity, modeled for neutral atmosphere (i.e. < 60 km) as,

$$N(z) = k_1 \frac{P(z)}{T(z)} + k_2 \frac{e(z)}{T^2(z)} \tag{1}$$

Where, refractivity (N), temperature (T) & pressure (P) and water vapor partial pressure (e) are the functions of altitude (z); $k_1 = 77.6 K/mb$ and $k_2 = 3.73 \times 10^5 K^2/mb$ [24]. The full expression for the refractivity for the entire atmosphere contains in addition to expression (1), the term due to free electrons in the ionosphere, and particulates (primarily, liquid water) [22]. For the "dry" part of the neutral atmosphere, the contribution of water vapor pressure is generally negligible, causing the refractivity, expressed in expression (1), to be re-modeled as,

$$N(z) = 77.6 \frac{P(z)}{T(z)} \tag{2}$$

If P(z) & T(z) represent the true atmospheric state vectors, the Right Hand Side (R.H.S.) term of expression (2) will very closely approximate the total refractivity N(z) on the Left Hand Side (L.H.S.) for z > z1; the threshold z1, generally, being ~12-14 km in the tropics and 6-8 km in the middle and higher latitudes. However, this equality will not hold for z < z1, as the R.H.S. doesn't account for the extra refractivity contribution from the second term of (1). The extra contribution from the water vapor term (or, the "wet" term) of refractivity (expression 1) is positive and inherent in the total refractivity. Thus, if the total refractivity, N(z), is inverted to pressure and temperature on the R.H.S. in the absence of water vapour term, the inverted parameters will approximate very closely to the true state parameters for z > z1, but diverges, below this threshold, from its true value proportionately so that while the inverted pressure ($P_d$ (z)) exceeds the true pressure, the inverted temperature ($T_d$ (z)) decreases compared to the true temperature. The inverted temperature (hereafter, the "dry" temperature) will therefore show a cold bias and the inverted pressure (hereafter, the "dry" pressure) a warm bias with respect to their true counterparts for z < z1. This is illustrated in figure 1. With the statistical characteristics of the "dry" parameters outlined through the discussion presented above, the next sub-section gives the detailed retrieval procedure for the "dry" atmospheric parameters.

## 2.1 "Dry" Atmospheric Retrievals

The expression (2) can be re-written in terms of the "dry" pressure ($P_d$ (z)) and "dry" temperature ($T_d$ (z)) as,

$$N(z) = 77.6 \frac{P_d(z)}{T_d(z)} \tag{3}$$

The density profile ($\rho(z)$) is related to N(z) by the expression

$$N(z) = 77.6 R(\rho_d(z) + \rho_w(z)) \tag{4}$$

where, the total density $\rho(z)$ is the sum of the "dry" air density $(\rho_d(z))$ and the moist air density $(\rho_w(z))$. Expression (5) results from substituting for volume from the ideal gas equation PV=RT for 1mole of gaseous air.

$$\rho_d(z) + \rho_w(z) = \frac{m_d.P(z)}{T(z).R} + \frac{(m_w - m_d).e(z)}{T(z).R} \tag{5}$$

$R$ is the gas constant, $m_d$ and $m_w$ are the molecular mass of dry air and water vapor, respectively. The hydrostatic expression, after substituting (4) & (5) for the total density, has the form

$$\frac{dP(z)}{dz} = -g\rho\rho(z = g\frac{m_d.N(z)}{k_1R} + \frac{k_2gm_d.e(z)}{k_1.R.T^2(z)} + g\frac{(m_d - m_w).e(z)}{R.T(z)} \tag{6}$$

The "dry" pressure ($P_d(z)$) is retrieved by integrating the expression (6) after ignoring the 2nd and 3rd terms on the R.H.S and is expressed as

$$P_d(z) = \frac{m_d}{k_1 R_d} \int_z^\infty g(z').N(z')dz' ,$$ (7a)

where, $R_d$ (=287.0 J/K/Kg) is the gas constant for dry air. The integration ideally extends to infinity i.e. up to the top of the atmosphere. The implicit addition to the R.H.S of (7a) is P(z=∞), which tends to zero as z tends to infinity. However, N is a known measurement only up to a finite height z = $z_u$, which for the neutral atmosphere, comprising of the troposphere, the stratosphere and the mesosphere, is 60 km. Information from MSIS-90 atmospheric climatology model extends the knowledge of N up to the height of 120 km. The model provides the profiles of temperature and total mass density as a function of geodetic latitude, longitude and altitude [25]. Choosing the upper limit of integration, $z_u$, to be 120 km has a practical advantage of mitigating the propagation effect of error in climatology to the region of interest i.e. below 60 km. The implicit pressure term, $P(z = z_u)$, known from the climatology data, is explicitly incorporated as,

$$P_d(z) = P(z = z_u) + \frac{m_d}{k_1 R_d} \int_z^{z_u} g(z').N(z')dz'$$ (7b)

(7b) is solved numerically for the "dry" pressure which is substituted in (8) to simultaneously solve for the "dry" temperature, given as,

$$T_d(z) = \frac{77.6}{R_d.N(z)} P_d(z) = \frac{77.6}{R_d N(z)}[P(z = z_u) + \frac{m_d}{k_1 R} \int_z^{z_u} g(z').N(z')dz']$$ (8)

The cold bias in "dry" temperature, as discussed in section 2, is evident from figure 1 (left panel; black line) for the altitudes below ~10 km, where the correction for the water vapor term yields the true temperature (shown by the red line). Both the "dry" and the true parameters are retrieved from COSMIC refractivity using our algorithm and is shown for illustration of cold and warm biases in "dry" temperature and "dry" pressure, respectively w.r.t. their true counterparts in the presence of humidity in the lower troposphere. Above 10km (for this case), the true temperature is as good as the "dry" temperature. Conversely, the "dry" pressure has a warm bias vis-a'-vis its true counterpart below 10 km (fig.1; right panel). Bias in pressure is less prominent than that for the temperature because of its lower sensitivity to the water vapor correction as a ratio of its absolute magnitude, which increases exponentially with decrease in altitude.
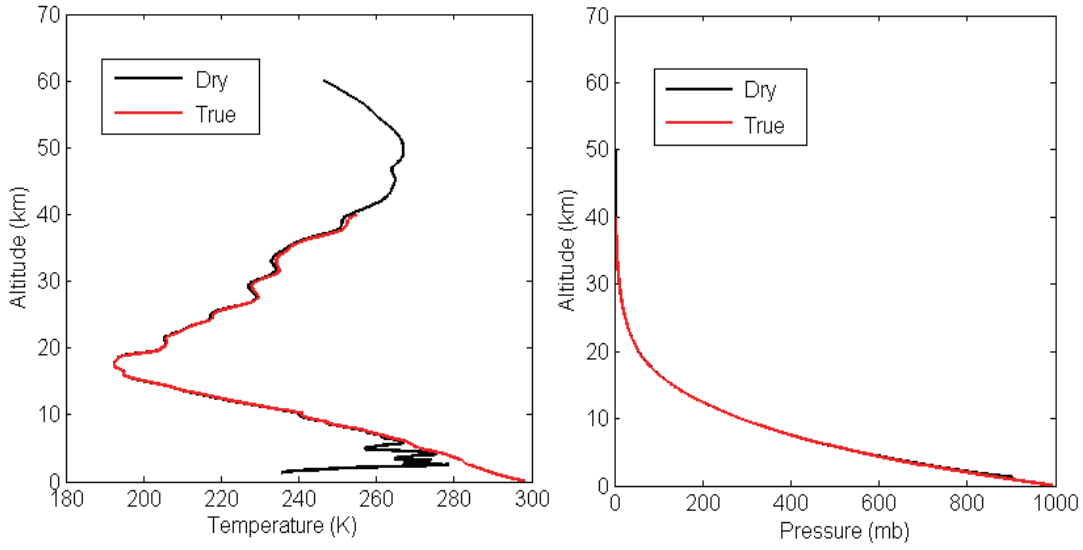
**Figure 1.** Illustrative plots of "dry" temperature (left panel) and "dry" pressure (right panel) with their true counterparts for a particular COSMIC occultation event.

The "dry" temperature is more sensitive to refractivity than the "dry" pressure due to the presence of the term $N(z)$ outside the integration in (8). Error in refractivity has, therefore, a higher impact on "dry" temperature. Figure 2 shows the temperature (upper panel) and water vapor partial pressure (lower panel) sensitivity to refractivity. The "dry" temperature sensitivity is shown above 10-12 km for changes in $N(z)$ from 1% - 5%. The absolute change in $N(z)$ is shown by dashed lines of different colours. It may be inferred that 1% change in $N(z)$ results in nearly 2-3 K change in "dry" temperature at all levels and 5% will affect the temperature by 14-15 K at 60 km. A 1% change in refractivity causes an absolute change of water vapor partial pressure to less than 1 mb near the Earth's surface and less than 0.1 mb at 20 km. This follows for the rest of the cases and is due to decreasing presence of water vapor in the upper troposphere. Thus, above 20-25 km, where water vapor presence is hardly observed or is in trace amount, temperature is more sensitive to refractivity as seen from the higher change in it beyond 20 km. The rareness of the atmospheric density at higher levels beyond 20 km and the inverse proportionality to refractivity explains physically the higher sensitivity of inverted temperature at higher levels. Further, positive change in refractivity results in negative change in temperature, whereas it is unidirectional for water vapor partial pressure. [26] have shown conversely the sensitivity of fractional difference in refractivity with changes in temperature, pressure, water vapor partial pressure and relative humidity for a particular day occultation event from COSMIC and radiosonde data.
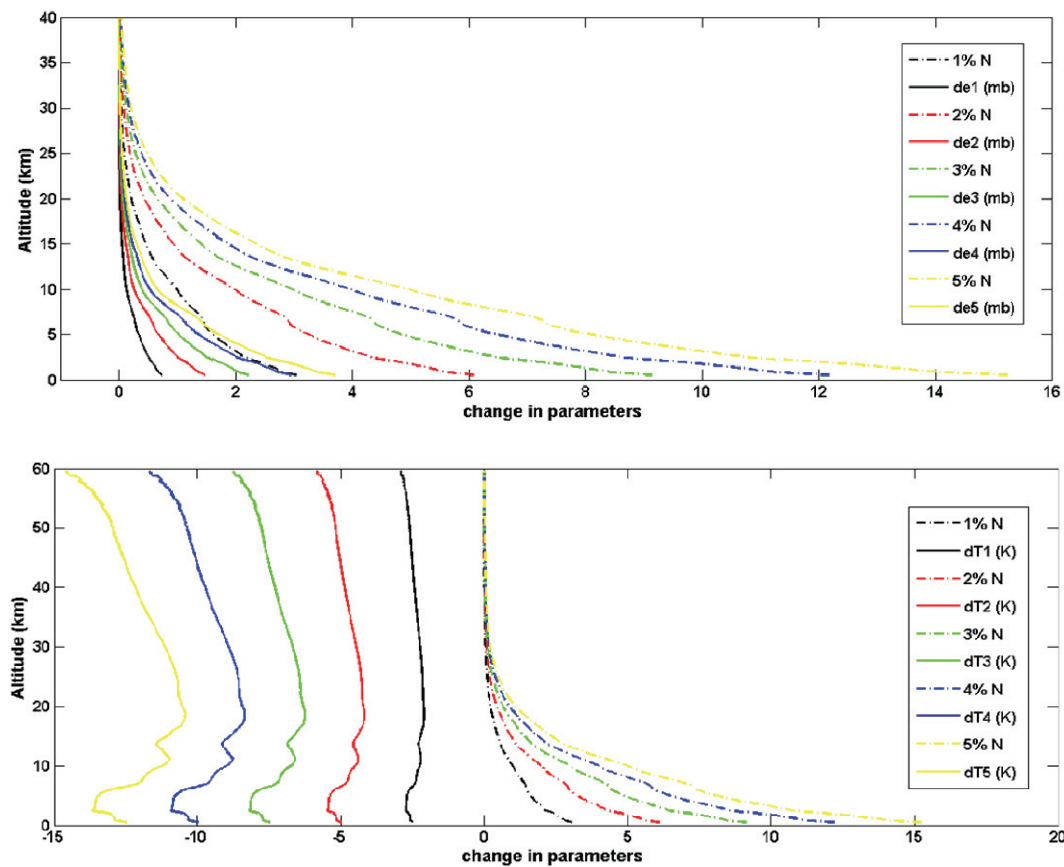
**Figure 2.** Sensitivity of temperature (upper panel; solid lines) & water vapor partial pressure (lower panel; solid lines) to percent change in refractivity (upper & lower panels; dashed lines).

## 2.2 "Wet" Retrieval

The demarcation between the "dry" and the "wet" part of the atmosphere depends on the height below which the water vapor contribution cannot be ignored. This height may be termed as the water vapor point [23], [27], hereafter abbreviated as *wvp*. A valid determination of the *wvp* must account for the highly dynamic nature of the vertical profile of water vapor concentration as a function of geo-location and time. [27] assumed the *wvp* for which the maximum possible temperature error due to water vapor partial pressure is 2 K. Further, this assumption was based on worst error scenario for GPS/MET RO mission, which stood at 2 K. However, below this *wvp*, the temperature error for a saturated atmosphere could be larger than 2 K [27].

A distinct approach to select the *wvp* should be based on a realistic assessment of the statistical errors in retrieved temperature, pressure and humidity profiles through a sensitivity study performed over a set of *wvp*. [28] describes in detail the approach as well as the results of the sensitivity study using a diverse set of Thermodynamic Initial Guess Retrieval (TIGR) radiosonde (both humid and less humid cases) as well as COSMIC data for the tropical region. For clarity and completeness sake, the approach and the conclusion is summarized in the next sub-section.

**2.3. Selection of Water Vapor Point (wvp)**

The demarcation height is parameterized in terms of temperature, which is advantageous as the vertical variation of water vapor in the atmosphere is correlated with the temperature variation. This ensures that the *wvp* is dynamically assigned for each occultation event. A reference water vapor point is selected at 230 K and a set of eight distinct water vapor points ranging from close to tropopause (~3 km above the reference water vapor point) to close to 8 km (~2 km below the reference water vapor point), is considered corresponding to heights which generally varied from one occultation event to another. 5040 diverse profiles of TIGR radiosonde, covering 30S-30N and spanning a period of over a decade, were taken for the sensitivity study. In addition, the sensitivity was also carried out on realistic observations from 663 COSMIC profiles over 10S-30N region during May-September 2006. Temperature, pressure and humidity were retrieved from refractivity simulated from each of the 5040 TIGR profile by application of the retrieval approach, as discussed in sub-section 2.1 and 2.4, for each of the *wvp* from the chosen set. The mean difference and root mean square error in temperature, pressure and humidity retrievals were compared for all the nine cases of *wvp*. It was inferred that the reference water vapor point (at 230 K of "dry" temperature) is relatively suitable for demarcation of the "wet" and "dry" atmosphere, although higher *wvp* (close to 13.6 km) yielded temperature mean deviation of 0.5 K and root mean square deviation (rmsd) of 2.1 K at broadly all levels up to 14 km but with a much higher pressure mean deviation of -1.5 mb and rmsd of 2.1 mb at 7 km. With reference *wvp*, the temperature mean deviation peaks to 1.5 K (2.0 K) and has an rmsd of 2 K (2.2 K) at 4 km for the non-humid (humid) case. Humidity retrieval with reference *wvp* showed peak mean deviation of only 0.2 g/kg (0.3 g/kg) and rmsd of 0.3 g/kg (0.35 g/kg) at about 4 km for the non-humid (humid) case. The reference water vapor point performed equally well for COSMIC dataset. Hence, we have chosen a dynamic criterion for *wvp* estimation to correspond to the parametric height at 230 K isotherm in the retrieved "dry" temperature profile.

**2.4 Description of the "Wet" Retrieval**

The approach followed in this paper for "wet" retrieval is based on the works presented in detail in [27]. The important assumption is that temperature can explicitly be assumed to be related quadratically to natural logarithm of pressure. The validity of this assumption, not shown in the previous work, is tested with two available in-situ datasets viz. NCEP analyses and radiosonde data. The scatterplot is shown for radiosonde in figure 3 (left panel) and for NCEP in figure 3 (right panel). The x-axis contains the in-situ temperature and the y-axis shows the temperature obtained from quadratic fit to the natural logarithm of pressure. The correlation coefficient, r, is more than 0.9 in both the plots of figure 3, implying that more than 81% of the variability is explained by the quadratic assumption, which is statistically significant to confirm the validity of the above-stated temperature quadratic assumption. For the sake of completeness of the discussion in this paper, it is pertinent to discuss the steps of the implemented algorithm.
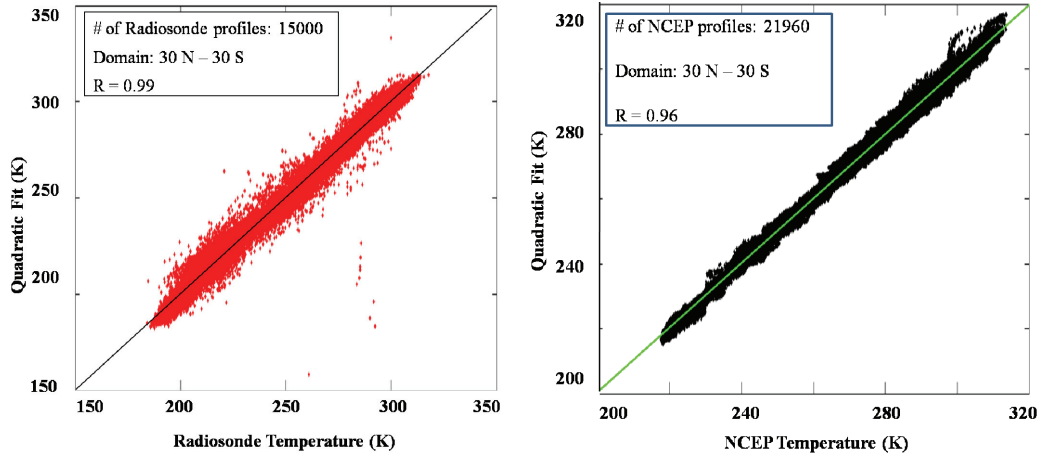
**Figure 3.** Scatterplot of temperature from quadratic fit with in-situ temperature from Radiosonde (left panel) and NCEP analyses (right panel).

The temperature quadratic in natural logarithm of pressure can be mathematically formulated as,

$$T(\eta) = a + b \bullet \eta + c \bullet \eta^2 \tag{9}$$

where, $\eta = \log_e(P)$ is the natural logarithm of pressure, P and a, b & c are the unknown quadratic coefficients to be computed simultaneously from the three algebraic expressions as follows,

i) 
$$T(\eta_s) = a + b \bullet \eta_s + c \bullet \eta_s^2 \tag{10a},$$

where $\eta_s$ is the natural logarithm of pressure taken at the surface and $T(\eta_s)$, the corresponding temperature at the surface. The two surface parameters are the auxiliary information to the retrieval algorithm which can be sourced from any reliable dataset. To allow for the availability of this information at the location of an occultation event, which are rather known to be random, a practicable solution is to consider gridded NWP dataset. Within the constraints of operational necessity, the timely availability of forecast dataset in real-time scenario may often not be possible and therefore it was considered to work with mean surface temperature and pressure from NCEP analyses data for the years 2010-2012. Statistically, the monthly rmsd of surface parameters from the mean is evaluated for all the months, shown in figure 4 for the months of January and June only, to reveal the largest possible variability expected from the use of the mean surface values. Between 35N-35S, the tropical surface temperature is more or less invariable with a maximum change of 0.4-0.8 K in most of the regions, except at the northern periphery with variations of up to 1.2 K. This trend is observed for both the months, representing
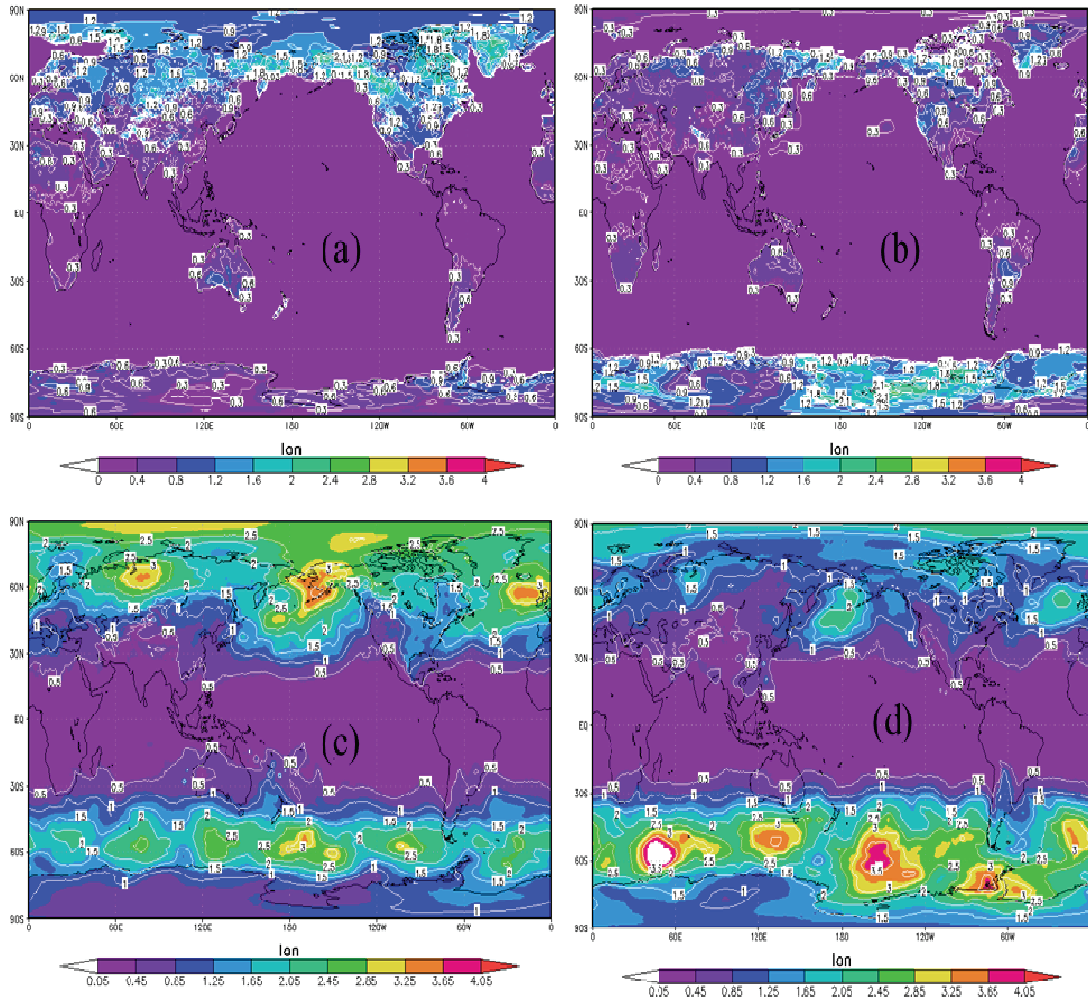
**Figure 4.** RMSD of surface temperature (a & b) and pressure (c & d) from NCEP analyses for the months of January (a & c) and June (b & d).

peak summer and winter conditions (figs. 4a & b). Surface pressure also has a uniform rmsd of as high as 0.05 mb within 30N-30S in both the months (figs. 4c & 4d). Non-uniform variability is noticeable beyond 30° in both the hemispheres with maximum of up to 2.45 mb. Inferentially, seasonality has minimal yet non-negligible impact on the rmsd of the surface parameters. Therefore, to account for such seasonal changes, howsoever small, a monthly database of mean surface temperature and pressure is prepared from 2010-2012 analyses of NCEP as the auxiliary dataset.

ii)
$$T(\eta_{wvp}) = a + b \bullet \eta_{wvp} + c \bullet \eta_{wvp}^{2}$$
(10b),

where $\eta_{wvp}$ is the natural logarithm of pressure selected at the *wvp* and $T(\eta_{wvp})$, the corresponding temperature at the *wvp*. As suggested by [27], the temperature and pressure at the *wvp* are assumed to be the derived "dry" parameter values. The *wvp* itself located using the criterion of 230 K isotherm in the "dry" temperature profile.

iii) The third expression is obtained by combining the hydrostatic expression with ideal gas law, yielding

$$\int_{\eta_s}^{\eta_{wvp}} T(\eta)d\eta = -\int_{z_s}^{z_{wvp}} \frac{g}{R_{air}}dz \tag{10c}$$

where z refers to the geopotential height (in km units), g, the acceleration due to gravity (in m/s$^2$) as a function of height and latitude and $R_{air}$, the gas constant of air (in J/kg/K). In the beginning, as we do not have knowledge of water vapor, $R_{air}$ may be substituted with $R_{dry}$. $T(\eta)$ is replaced by the assumed quadratic expression and the quadratic coefficients a, b and c are computed by simultaneously solving the three expressions (10 a, b & c). With the known coefficients, the first cut temperature profile is estimated using the "dry" pressure profile between the surface and the *wvp*. Subsequently, the first estimate of water vapor partial pressure is calculated using the expression,

$$e = \frac{T^2 N - 77.6PT}{3.73 \times 10^5} \tag{11}$$

Using the first estimate of water vapor partial pressure, the mixing ratio (w), given by

$$w = 0.622 \frac{e}{P} \tag{12}$$

and the virtual temperature ($T_v$) profile is calculated using the formula

$$T_v = \frac{T(1.0 + (1.61 * w))}{(1.0 + w)} \tag{13}$$

The pressure profile is refined from the initialized "dry" pressure profile by feeding the virtual temperature profile into the hydrostatic expression,

$$P = P_{wvp} \exp\left(-\int_{z_{wvp}}^{z} \frac{g}{R_{dry}T_v}dz\right) \tag{14}$$

The re-estimated pressure from (14) is used to refine the temperature quadratic (9) and repeat the sequence from (9) to (14) until the set convergence criterion is reached. The convergence criterion in our algorithm is set as the upper limit on the incremental average pressure change between two successive iterations. Simultaneously, in order to restrict to realistic iteration counts, an upper limit is also set on the number of allowed iterations within which to converge. Generally, such a limit is set to 10, although in maximum cases, it has been observed to converge in 4-5 iterations. Figure 5 shows the iterative convergence of a sample retrieval of temperature, pressure and water vapor partial pressure which has converged in three iterations. Chances of non-convergent scenarios are likely to crop up when the initialization is far away from the realistic values. Such cases have fortuitously not been encountered with the carefully constructed database of auxiliary dataset of surface parameters and the *wvp* threshold of 230 K. We note that two options are possible during the iterations (not pointed out by [27]): (i) keep the coefficients of temperature quadratic same throughout the iterations with $R=R_{dry}$ approximation in expression (14) and (ii) update the right hand

side integral in expression (14) with water vapor information and hence solve for fresh temperature quadratic coefficients in each iteration which requires refractivity profile to be available up to the surface or lower altitude. In our algorithm, we follow the first approach only as radio occultation derived refractivity profile do not reach the surface and are often available only up to altitudes of 1 km and above. Also, knowledge of near surface refractivity requires information on surface humidity and hence, in practice, the second option is not feasible.
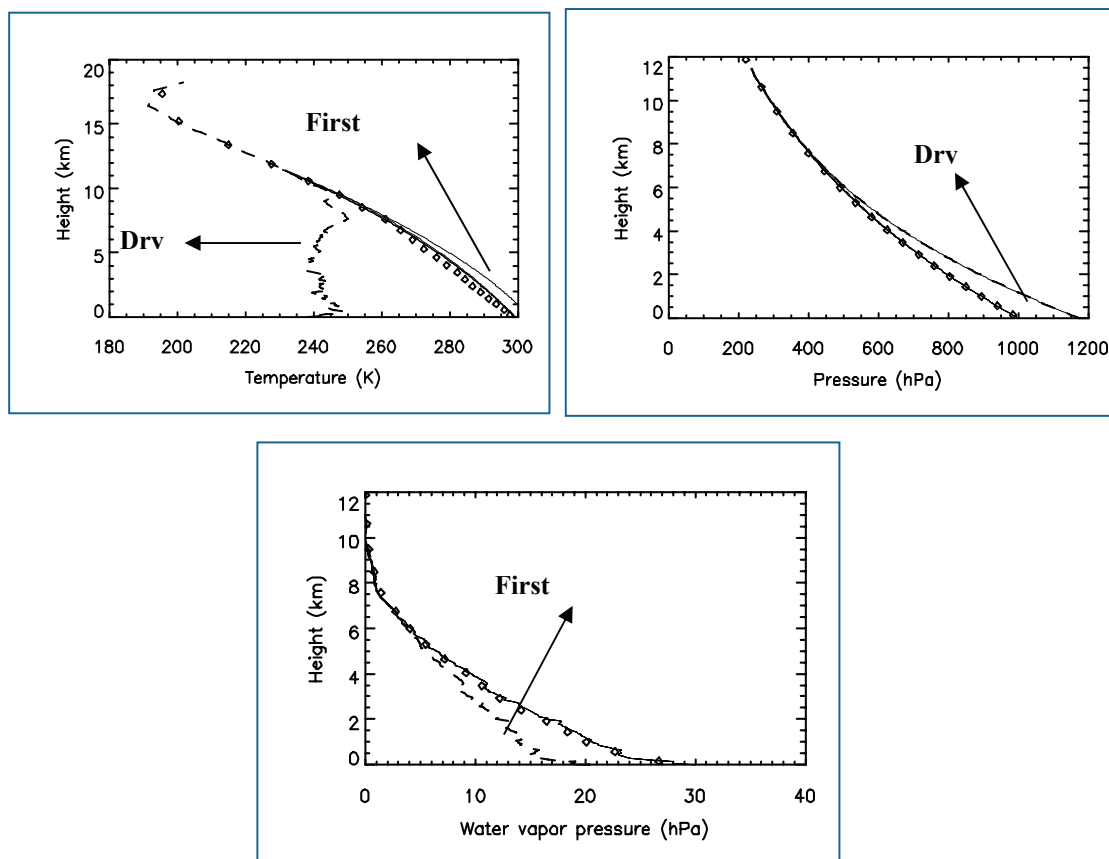


**Figure 5.** Illustration of iterative convergence of temperature, pressure and water vapor pressure for a sample case. "Dry" parameters are seen to deviate below ~12km (the water vapor point for this case).

The input to the retrieval algorithm is refractivity profile (in this paper, from NCEP simulations and COSMIC), altitude and geo-location information. Retrieval is set on for only those profiles which pass the gross quality checks – the range check for refractivity- to take care of the N-bias problem (more discussions in sub-section 4.2) and, other metadata such as the latitude, longitude and time; diagnostic check for missing refractivity at various vertical levels as well as bulk missing cases. In order that the file is selected for onward processing, at least 50% of the levels must contain range-qualified refractivity data. With the use of upper air climatology, "dry" parameters are estimated; the "dry" temperature further used for the location of *wvp*.

If the occultation sounding penetrates substantially below the *wvp,* "wet" retrieval is triggered and final geophysical profiles are retrieved with the help of mean surface auxiliary database. If not, the final output contains only the profiles of "dry" parameter with relevant flag information.

## 3. Discussions on the "Dry" Retrieval

Figure 6 shows two cases of the "dry" retrievals of temperature and pressure from COSMIC refractivity data using the developed algorithm and their comparison with corresponding "dry" products (filename: 'atmprf') from COSMIC. COSMIC data available from http://tacc.cwb.gov.tw/cdaac/ are used for qualitative comparison and quantitative validation. For both the cases, the "dry" temperature and "dry" pressure match well with the COSMIC "dry" products with small deviation in temperature observed to occur progressively from 45-60 km. Further test of the accuracy of the "dry" retrievals vis-a'-vis the true atmospheric profiles of temperature and pressure, is done by computing statistical mean difference and standard deviation against COSMIC "wetprf" dataset (period 2011). It may be worthwhile to mention that the "wetprf" dataset contains, besides other parameters, the operational retrievals of atmospheric temperature, pressure and water vapor partial pressure profiles using the 1DVAR technique.
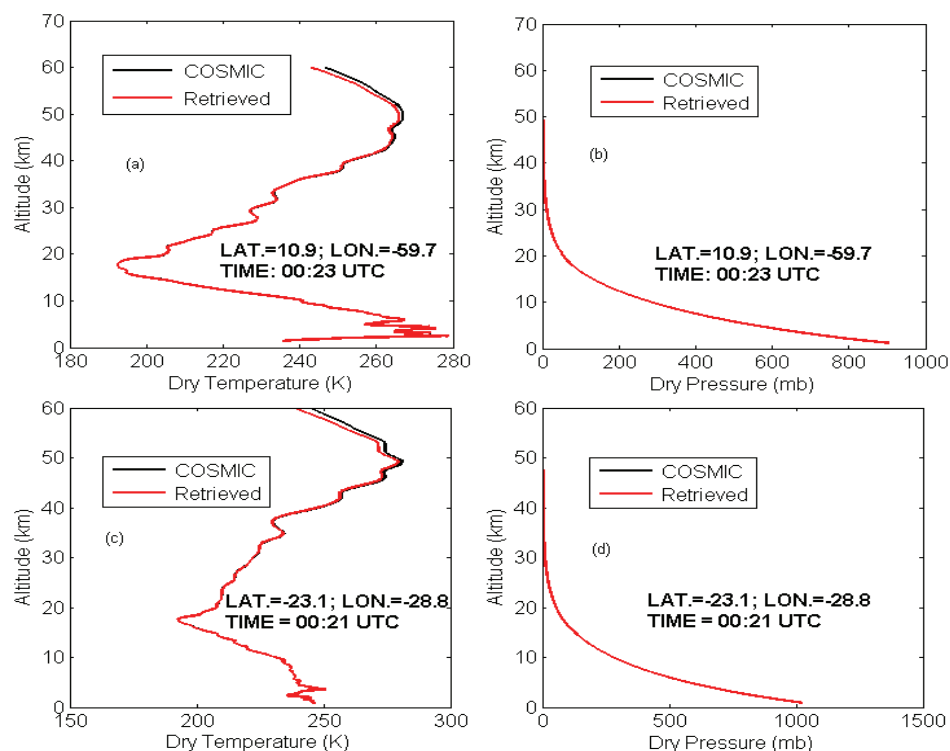


**Figure 6.** Two examples of "dry" retrievals from COSMIC refractivity for the shown spatio-temporal geolocation using the in-house algorithm and compared with COSMIC "dry" retrieval products.

The mean difference in "dry" temperature and pressure is insignificant beyond 14 km (fig.7 (a), (b); solid lines) during all the four seasons: Winter (DJF), Spring (MAM), Summer (JJA) and Autumn (SON). Below 14 km, the systematic bias in "dry" parameters due to neglect of humidity information results in relatively large deviation from the true atmospheric state. The standard deviation (dashed lines) of "dry" temperature (fig. 7 (a)) and "dry" pressure (fig. 7 (b)) is within 0.7 K and 0.3 mb, respectively, between 14-30 km. Below 14 km, the increase in standard deviation for both the parameters is expected as the difference between the "dry" and true profile is bound to be large when water vapor contribution is neglected in the region (i.e. lower tropical troposphere; below 12-14 km) where it happens to be dominant. Thus, the differences below 14 km as shown in figure 7 (a & b) are illustrative of this fact. However, the
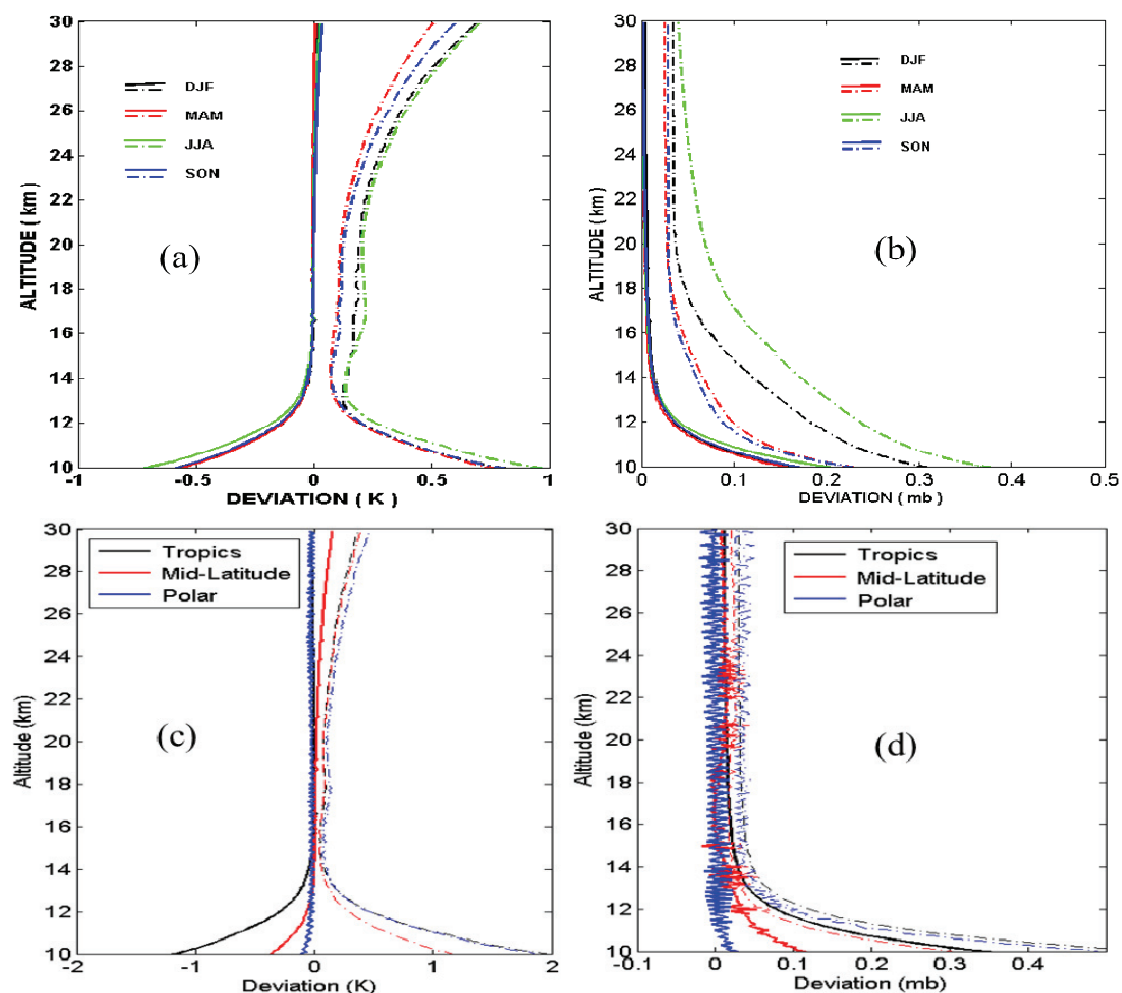


**Figure 7.** Mean difference (solid line) and standard deviation (dashed line) of (a), (c) "dry" temperature and (b), (d) "dry" pressure retrieved from COSMIC refractivity (2011 data) with respect to COSMIC 1DVAR retrievals (true profiles) for (a), (b) different seasons, and (c), (d) different geographical regions.

deviations above 14 km in both the parameters suggest that the "dry" retrievals are not exactly coincident compared to COSMIC 1DVAR retrievals. This may also happen due to the use of climatology data for the initialization of the hydrostatic integral in the estimation of "dry" parameters, unlike the COSMIC 1DVAR retrievals which uses Bayesian technique to obtain the optimal solution. Similar deviation is also seen, not shown in this paper, between COSMIC "dry" parameters (from 'atmprf' files) and COSMIC 1DVAR retrievals (from 'wetprf' files). Figures 7 (c) & (d) show the mean difference and standard deviation of the retrieved "dry" temperature and "dry" pressure with respect to COSMIC 1DVAR retrievals for the three geographical regions- tropics, mid-latitude and polar. The mean difference for "dry" temperature is negligible above 14 km (tropics), 12 km (mid-latitude) and 10 km (polar) and the standard deviations beyond 14 km are within 0.5 - 0.7 K for all the regions (fig. 7(c)). Both the mean difference and standard deviation of "dry" pressure are within 0.1 mb beyond 14 km (fig. 7(d)). The relative performance of the "dry" retrievals from our algorithm compared to corresponding COSMIC 1DVAR products is reasonably good in the dry portions of the atmosphere in different geographical regions. Deviations are seen below 14 km for all the regions and for both the "dry" parameters because "dry" profiles, derived with the neglect of water vapor contribution in refractivity, are compared with the true profiles, having non-negligible contribution from the humidity in the atmosphere.

**4. Discussions on the "Wet" Retrieval**

The retrieval algorithm is applied to two different datasets. Firstly, we show the results of retrieval from simulated refractivity using NCEP analyses dataset (source: http://nomads.ncdc.noaa.gov) in sub-section 4.1. The next sub-section illustrates the direct application on COSMIC observations and the comparison against collocated radiosonde. Simultaneously, the statistical bias and standard deviation of COSMIC 1DVAR retrievals against the collocated radiosonde are also presented. The statistical comparison is done for global datasets as well as for tropics separately.

*4.1 Simulation Results*

Simulated refractivity data was prepared from NCEP gridded atmospheric profiles of temperature and water vapor partial pressure (converted from relative humidity contained in the NCEP file) at defined pressure levels spanning from near surface to 30 km. For each of the 27000 COSMIC occultation events, temperature and humidity profiles from the four nearest gridpoints were interpolated 4-dimensionally in latitude, longitude, height and the time dimension to get a common temperature and humidity profiles at the location of the corresponding COSMIC event. Pressure interpolation is done by considering pressure as a function of height for the considered four gridpoints in the NCEP data which is first interpolated to the common location of the COSMIC event and then interpolated at the given heights in the COSMIC data. Interpolated temperature, pressure and humidity profiles are forward modeled using expression (1)

to get the realistic occultation type profiles of refractivity. The interpolated temperature and humidity at the location of COSMIC event are the standard dataset for comparison. The simulated refractivity is extrapolated to a height of 120 km by using collocated MSIS-90 climatology [25] on top of the NCEP simulation data. This is necessitated by the hydrostatic integral initialization for the "dry" parameters' retrieval. Subsequently, "wet" retrieval is performed for heights below 230 K isotherm in the "dry" temperature. Figure 8 shows the mean difference (solid line) and standard deviation (dash-dotted) for the retrieved temperature (top left panel) and water vapor partial pressure (bottom left panel). The lower panel of figure 8 show the number of collocated data at various heights for temperature (solid line) and water vapor partial pressure (dash-dotted), respectively. Sharp fall in collocation numbers below 5 km is primarily due to varying lowest heights of penetration in COSMIC data for which the simulated refractivity dataset has been prepared.
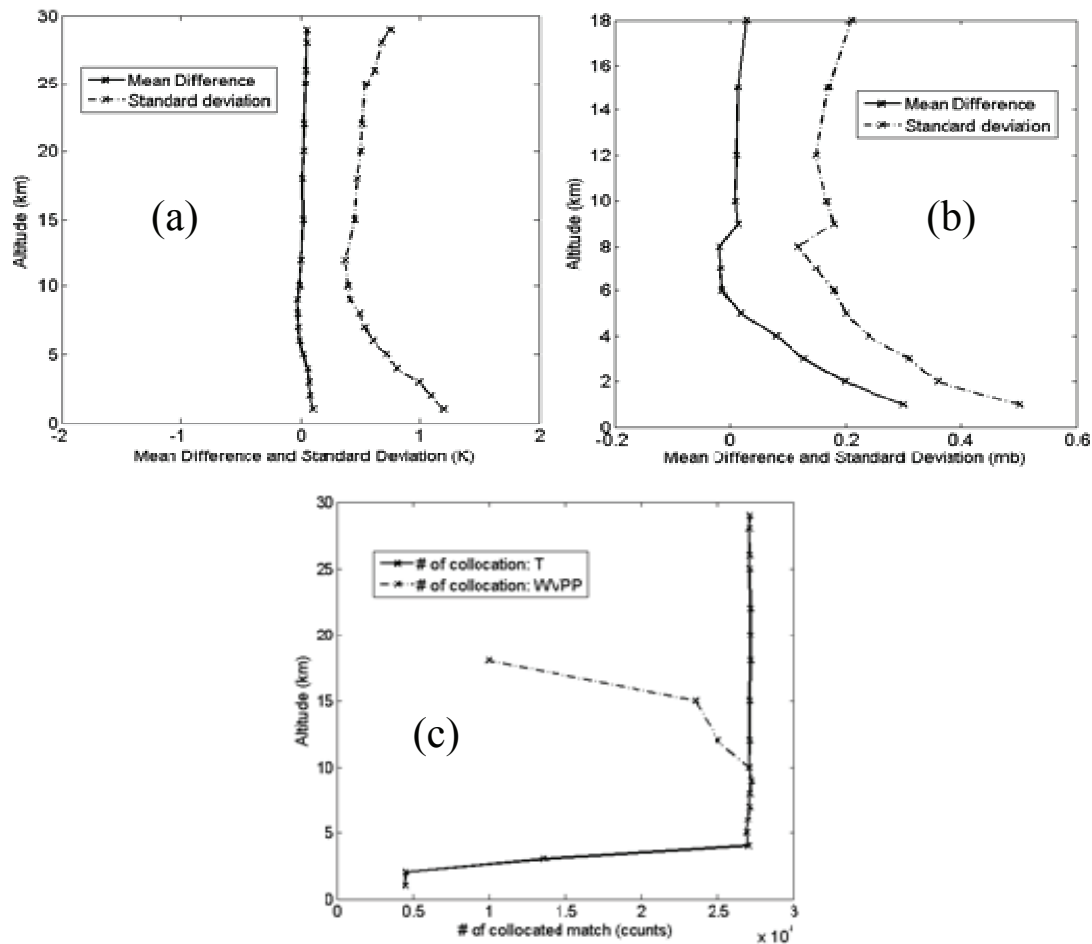


**Figure 8.** Mean difference (solid line) and standard deviation (dash-dot line) of temperature (left panel; top) and water vapor partial pressure (right panel, top) retrieved from NCEP-simulated refractivity w.r.t. NCEP analyzed products. Number of collocated pairs for temperature (solid) and water vapor partial pressure (Dash-dot line) is shown (bottom).

The mean difference of temperature is within ±0.2 K between 1-30 km. After correcting for the bias, the standard deviation is within 1 K from 3-30 km. Below 3 km, it shows a peak value of 1.2 K at 1 km. The mean difference and standard deviation of water vapor partial pressure fall off nearly exponentially with height with peak values of 0.32 mb and 0.55 mb at 1 km, respectively.


## 4.2 Retrieval from COSMIC Refractivity and Validation

The algorithm is applied on COSMIC refractivity profiles (from 'atmprf' files; year 2011). It is important to note that some of the COSMIC refractivity profiles show large systematic negative refractivity bias (commonly referred to as N-bias) which are much more common in the tropics. A significant number of occultations in the tropics, however, show little or no bias, but, a few strongly biased occultations deteriorate the mean fractional refractivity difference [29]. [29] show that large negative N-bias, present in CHAMP & SAC-C data, above 2 km are removed by solving multipath propagation problem using wave optics retrieval of bending angle. This is also true for COSMIC data where wave optics retrieval is implemented for multipath cases [30]. Below 2 km, the negative N-bias problem persists in COSMIC refractivity data. To remove the large negative N-bias effects of these few outliers, a quality control of refractivity data is done at the retrieval stage, as discussed in sub-section 2.4. Occultation events with refractivity profile exceeding 0-370 N-units are flagged out and discarded at the retrieval stage. These may be referred to as quality-controlled refractivity profiles. However, some of the refractivity profiles within the specified quality range, but with negative N-bias, could still intrude into the retrieval chain and contribute to bias in retrieved temperature and water vapor partial pressure. Rigorous specification of refractivity quality range at each vertical level and for each latitude-longitude bin is required as a further quality check. We have not accounted for it in this work as it requires a separate climatological study for refractivity profile across the globe. Figures 9 (a-b) show the results of validation of the temperature and water vapor partial pressure retrieved from quality-controlled refractivity profiles with respect to collocated radiosonde. Simultaneously, operational 1DVAR retrievals for the same set of quality-controlled dataset of COSMIC are compared statistically against the collocated radiosonde (figs. 9 (c-d)). The 1DVAR profiles (from 'wetprf' files) are available at the mean sea level altitudes with uniform spacing of 100 m from 0 – 39.9 km. However, the radiosonde data are available at lesser vertical samples and up to a maximum height of 30 km, in general. Accordingly, after collocation, both the datasets are interpolated at a common vertical interval of 500 m up to a top altitude of 30 km.
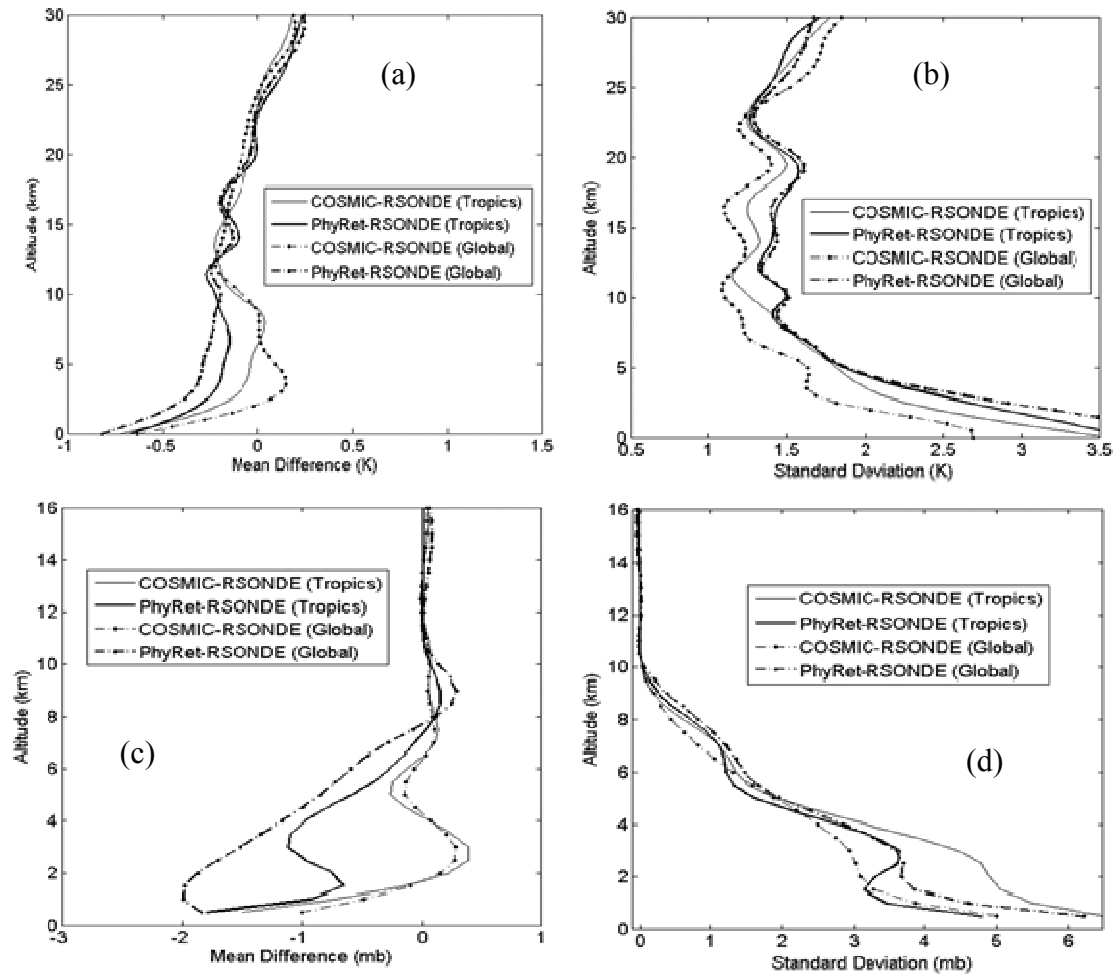
**Figure 9.** Mean difference (a, c) and Standard deviation (b, d) of temperature (a, b) and water vapor partial pressure retrieved from COSMIC refractivity w.r.t. collocated radiosonde for tropics (thick solid line) and globally (thick dash-dot line). Comparison for COSMIC operational 1DVAR products w.r.t. the collocated radiosonde is also shown for the tropics (thin solid line) and globally (thin dash-dot line).

For comparison, tropical events have been segregated from the global dataset. The statistics for the former are shown with solid lines whereas dash-dotted lines depict the same for the global dataset. Further, the thick lines are used for comparison of physical retrieval method (or, PhyRet for discussions hereinafter) and thin lines for comparison of COSMIC 1DVAR products (now onwards 'COSMIC') with respect to collocated radiosonde. These line-types have been followed in all the figures from figure 9 onwards. The radiosonde data for validation are the collocated files ('sonprf') from TACC centre (http://tacc.cwb.gov.tw/cdaac). These files contain profiles of temperature, pressure, water vapor partial pressure, refractivity and mean sea level geometric height apart from the global attributes such as time, latitude, longitude and the spatio-temporal separation of the radiosonde from the collocated COSMIC

occultation event. We have selected the collocation window of 3 hours and 300 km between COSMIC and radiosonde for validation purpose. Above 5 km, the mean difference and standard deviation of temperature are within -0.35 K to 0.25 K and 1.8 K, respectively, for both the tropics and the global dataset. Below 5 km, the mean difference and the standard deviation increase in the range of -0.5K to -0.75 K and 2.75 K to 3.5 K, respectively (figs. 9 (a-b)). The PhyRet and the COSMIC are reasonably close in terms of their mean differences against the radiosonde from the altitude range of 11-30 km. Below ~11 km, the mean differences are sensitive to the two methods over the two geographical datasets: tropics and the global, with peak differences between the two methods of 0.45 K (global) and 0.2 K (tropics) at 3.5 km and 8 km, respectively. Overall, the standard deviation is within 2 K in the altitude range of 5 – 30 km with COSMIC showing the least standard deviation from the lowest height to 22 km on the global dataset. COSMIC performance degrades in the tropics with peak value of 3.3 K at 0.5 km. PhyRet show less sensitivity between the tropics and global scenario, particularly, between 4 – 22 km with wider differences on the lower and upper side of this altitude range. Moreover, above 5 km, PhyRet differs from the COSMIC by as much as 0.5 K.

In figures 9 (c-d), water vapor partial pressure statistics are shown for PhyRet and COSMIC vis-a'-vis radiosonde. Sensitivity of the two methods is less pronounced between 8 – 16 km. Below this altitude range, significant differences are seen between the methods over the two geographical datasets. Mean differences are within -1 mb (COSMIC) and -2 mb (PhyRet). Between the two geographical datasets, PhyRet shows better result in tropics (-0.8 mb) than in global (-2.0 mb) at the altitude of 1.8 km (fig. 9c). Standard deviations are within 2.5 mb above 5 km for both the methods in both the geographical regions (fig. 9d) and are reasonably close to each other. At 2 km, PhyRet show better standard deviation of 3.2 mb than the COSMIC which is at 5 mb.

The differences in temperature and water vapor partial pressure (figures 9 (a-d)) provide an estimate of the relative performance of the PhyRet algorithm and a similar performance of COSMIC with respect to radiosonde as the reference dataset. It is evident that the PhyRet algorithm performs reasonably well and meets the current requirements of temperature accuracy of better than 2 K and water vapour standard deviation of less than 2.5 mb above 5 km. Moreover, on various counts, PhyRet performs reasonably better in tropics.


## 5. CONCLUSIONS

A retrieval technique based on physical iterative method is developed and the results of its application on simulation data of refractivity from NCEP analyses and over COSMIC operational refractivity products are presented and discussed in this paper. Simulation results show that the standard deviation (and, mean difference) is largely within 1 K (and, ±0.2 K) for temperature and up to 0.55 mb (and, 0.32 mb) for water vapor partial pressure above 1 km. Relative performance of the algorithm is demonstrated by applying it over COSMIC operational refractivity products and

comparing the retrieved parameters from PhyRet as well as those available as operational 1DVAR products from COSMIC with respect to radiosonde data as a common reference dataset. The validation statistics are shown for both the global region as well as for the tropics. Temperature profiles derived by PhyRet show a mean difference range of -0.19 K to 0.25 K and a standard deviation within 1.8 K in the tropics between the altitude range of 5 – 30 km. Global statistics show a small variation in the mean difference with a peak of -0.35 K at 5 km but is observed to be the same as in the tropics in terms of the standard deviation. COSMIC shows reasonably better standard deviation below 22 km with a range of 1.2 K (tropics) to 1.75 K (global) up to 5 km. The mean difference of COSMIC temperature in both the geographical regions are distinct and better than PhyRet below 10 km. Below 5 km, both COSMIC and PhyRet show increased values of mean difference and standard deviation, albeit, COSMIC performs relatively better than PhyRet in both the regions. COSMIC has however degraded accuracy in the tropics than over the whole globe. The performance deviations between PhyRet and COSMIC may be attributed to fundamental differences in the requirements of the two techniques- the physical iterative (our algorithm) and the 1DVAR (COSMIC). Two sources of deviations are the initialization of the hydrostatic integral and the use of surface data in physical iterative method, none of the two being used in 1DVAR. Considering further that we have used the collocation window of 300 km and 1 hour for collocating radiosonde data, these results compare well with the characteristic errors due to collocation mismatches between radiosonde and COSMIC retrievals shown in [31]. Water vapor partial pressure from our algorithm and from COSMIC 1DVAR also compares reasonably well with respect to collocated radiosonde fields between the altitude range of 8-16 km in the mean difference and between 4-16 km in the standard deviation. In figure 9c, below 8 km, PhyRet underestimates the water vapor pressure with respect to radiosonde in the mean sense, the deviation reducing in the tropics from the global mean value (-2 mb) by approximately 1 mb at 1 km. At the same height, COSMIC has a mean difference of -0.52 mb in both the regions. Below 4 km, the standard deviation of water vapour partial pressure exhibit pronounced variation for both the retrieval methods and in both the regions (fig. 9d). PhyRet performs better in tropics than COSMIC whereas COSMIC shows reasonably improved accuracy of water vapor partial pressure averaged globally. For temperature retrieval, PhyRet meets the global accuracy requirement of better than 2 K in the altitude range of 5 – 30 km, where the GPS-RO derived refractivity has shown the best accuracy. In this region, COSMIC has, however, the least standard deviation in the global average of better than 1.5 K at most of the vertical levels (fig. 9b). PhyRet is within 1.5 K at most of the vertical levels above 10 km with sporadic overshoots in between to a maximum of 1.8 K. Below 4-5 km, the accuracy of GPS-RO geophysical products suffers globally, more so, in the tropics and has been widely acknowledged in several literatures. Improvements in this region require an accurate estimation of refractivity in the boundary layer, which is an ongoing research problem in radio occultation worldwide [29], [30]. Such an improvement in refractivity would, in turn, require better receiver tracking with improved signal-to-noise ratio.

## ACKNOWLEDGEMENTS

## REFERENCES

[1] **Ware, R., M. Exner, D. Feng, M. Gorbunov, K. Hardy, B. Herman, Y. –H. Kuo, T. K. Meehan, W. Melbourne, C. Rocken, W. Schreiner, S. Sokolovskiy, F. Solhelim, X. Zou, R. A. Anthes, S. Businger and K. Trenberth,** 1996, "GPS sounding of the atmosphere from low earth orbit: preliminary results," *Bull. of Am. Meteorol. Soc.,* 77 (1), 19–40.

[2] **Escudero, A., A. C. Schleisier, A. Rius, A. Flores, F. Rubek, G. B. Larsen, S. Syndergaard and P. Hoeg,** 2001, "Ionospheric tomography using Oersted GPS measurements- Preliminary results," *Physics and Chemistry of Earth*, A 26 (3), 173-176.

[3] **Mostert, S. and J. A. Koekemoer,** 1997, "The science and engineering payloads and experiments on SUNSAT," *Acta Astronautica,* 41 (4-10), 401-411.

[4] **Wickert, J., C. Reigber, G. Beyerle, R. Konig, C. Marquardt, T. Schmidt, L. Grunwaldt, R. Galas, T. K. Meehan, W. G. Melbourne and K. Hocke,** 2001, "Atmosphere sounding by GPS radio occultation: 8rst results from CHAMP," *Geophysical Research Letters,* 28 (17), 3263–3266.

[5] **Hajj, G. A., C. O. Ao, B. A. Iijima, D. Kuang, E. R. Kursinski, A. J. Mannucci, T. K. Meehan, L. J. Romans, M. de la. T. Juarez and T. P. Yunck,** 2004, "CHAMP and SAC-C atmospheric occultation results and intercomparisons," *J. Geophys. Res.,* D06109, doi:10.1029/2003JD003909.

[6] **Wickert, J., G. Michalak, T. Schmidt, G. Beyerle, C. Z. Cheng, S. B. Healy, S. Heise, C. Y. Huang, N. Jakowski, W. Kohler, C. Mayer, D. Offiler, E. Ozawa, A. G. Pavelyev, M. Rothacher, B. Tapley and C. Arras,** 2009, "GPS radio occultation: Results from CHAMP, GRACE and FORMOSAT-3/COSMIC," T*err. Atmos. Ocean. Sci.,* 20(1), 35-50, doi:10.3319/TAO.2007. 12.26.01(F3C).

[7] **Anthes, R. A., P. A. Bernhardt, Y. Chen, L. Cucurull, K. F. Dymond, D. Ector, S. B. Healy, S. –P. Ho, D. C. Hunt, Y. –H. Kuo, H. Liu, K. Manning, C. Mccormick, T. K. Meehan, W. J. Randel, C. Rocken, W. S. Schreiner, S. V. Sokolovskiy, S. Syndergaard, D. C. Thompson, K. E. Trenberth, T. –K. Wee, N. L. Yen and Z. Zeng,** 2008, "The COSMIC/FORMOSAT-3 Mission-Early results," *B. Am. Meteorol. Soc.,* 89, 313-333.

[8]     **Engeln, A. von, Y. Andres, C. Marquardt and F. Sancho,** 2011, "GRAS radio occultation on-board of Metop," *Advances in Space Research,* 47, 336–347.

[9]     **Perona, G., R. Notarpietro and M. Gabella,** 2007, "GPS radio occultation on-board OCEANSAT-2 mission − An Indian (ISRO) and Italian (ASI) collaboration," *Indian J. Radio Space Phys.,* 36, 386 – 393.

[10]    **Beyerle, G., L. Grunwaldt, S. Heise, W. Kohler, R. Konig, G. Michalak, M. Rothacher, T. Schmidt, J. Wickert, B. D. Tapley and B. Giesinger,** 2010, "First results from the GPS atmosphere sounding experiment TOR aboard the TerraSAR-X satellite," *Atmos. Chem. Phys. Discuss.,* 10, 28821-28857, doi:10.5194/acpd-10-28821-2010.

[11]    **Bi, Y., Z. D. Yang, P. Zhang, Y. Q. Sun, W. H. Bai, Q. F. Dub, G. L. Yang, J. Chen and M. Liao,** 2012, "An introduction to China FY3 radio occultation mission and its measurement simulation," *Advances in Space Research,* 49, 1191–1197.

[12]    **Yunck, T. P., E. J. Fetzer, A. M. Mannucci, C. O. Ao, F. W. Irion, B. D. Wilson and Gerald John M. Manipon,** 2009, "Use of Radio Occultation to Evaluate Atmospheric Temperature Data from Spaceborne Infrared Sensors," *Terr. Atmos. Oceanic Sci.,* Vol. 20, Issue 1, 71-85.

[13]    **Leroy**, S. S., 1997, "Measurement of geopotential heights by GPS radio occultation," *J. Geophys. Res.,* 102, 6971–6986.

[14]    **IROWG,** 2017, "Report of the IROWG Activities: Outcome and Recommendations from the IROWG-5," *CGMS-45 IROWG-WP,* v2, 1-8, www.irowg.org.

[15]    **Fjeldbo, G. and A. J. Kliore,** 1971, "The neutral atmosphere of Venus as studied with the Mariner-V Radio Occultation Experiments," *The Astronom. J.,* 76 (no. 2), 123-140.

[16]    **Hajj, G. A., E. R. Kursinki, L. J. Romans, W. I. Bertiger and S. S. Leroy,** 2002, "A technical description of atmospheric sounding by GPS occultation," *J. Atmos. Sol. Terr. Phys.,* 64, 451-469.

[17]    **Poli, P., J. Joiner and E. R. Kursinski,** 2002, "1DVAR analysis of temperature and humidity using GPS radio occultation refractivity data," *J. Geophys. Res.,* 107(D20), 4448, doi:10.1029/2001JD000935.

[18]    **Palmer, P. I., J. J. Barnett, J. R. Eyre and S. B. Healy,** 2000, "A non-linear optimal estimation inverse method for radio occultation measurements of temperature, humidity and surface pressure," *J. Geophys. Res.,* 105, 17,513-17,526.

[19]    **Healy, S. B. and J. R. Eyre,** 2000, "Retrieving temperature, water vapour and surface pressure information from refractive index profiles derived by radio occultation: A simulation study," *Q. J. R. Meteorol. Soc.,* 126, 1661–1683.

[20] **Kursinski, E. R., S. B. Healy and L. J. Romans,** 2000, "Initial results of combining GPS occultations with ECMWF global analyses within a 1DVar framework," *Earth Planets Space,* 52, 885–892.

[21] **Kursinski, E. R., G. A. Hajj, K R. Hardy, L. J. Romans and J. T. Schofield,** 1995, "Observing tropospheric water vapor by radio occultation using the global positioning system," *Geophys. Res. Lett.*, 22, 2365– 2368.

[22] **Kursinki, E. R., G. A. Hajj, J. T. Schofield, R. P. Linfield and K. R. Hardy,** 1997, "Observing Earth's atmosphere with radio occultation measurements using the Global Positioning System," *J. Geophys. Res.,* 102 (no. D19), 23,429-23,465.

[23] **Jagadheesha, D., B. Simon, P. K. Pal, P. C. Joshi and A. Maheswari,** 2008, "A New Technique for Estimation of Lower-Tropospheric Temperature and Water Vapor Profiles from Radio Occultation Refractivity," *journal of atmospheric and oceanic technology,* 1075-1089, DOI: 10.1175/2008JTECHA1145.1.

[24] **Smith, E. K. and S. Weintraub,** 1953, "The constants in the equation for atmospheric refractive index at radio frequencies," *Proc. IRE,* 41, 1035-1037.

[25] **Hedin, A. E.,** 1991, "Extension of the MSIS Thermospheric Model into the Middle and Lower Atmosphere," *J. Geophys. Res.,* 96, 1159.

[26] **Rao, D. N., M. V. Ratnam, S. Mehta, D. Nath, S. G. Basha, V. V. M. J. Rao, B. V. K. Murthy, T. Tsuda and K. Nakamura,** 2009, "Validation of the COSMIC radio occultation data over Gadanki (13.488N, 79.28E): A tropical region," *Terr. Atmos. Oceanic. Sci.,* 20, 59–70.

[27] **O' Sullivan, D. B., B. M. Herman, D. Feng, D. E. Flittner and D. M. Ward,** 2000, "Retrieval of Water Vapor Profiles from GPS/MET Radio Occultations," *Bull. Amer. Met. Soc.*, 81 (no. 5), 1031-1040.

[28] **Shyam, A., P. C. Joshi and D. Jagadheesha,** 2009, "Sensitivity studies in the retrieval of geophysical parameters from radio occultation derived refractivity," *IITP-18, ISRO-Report.*

[29] **Ao, C. O., T. K. Meehan, G. A. Hajj, A. J. Mannucci and G. Beyerle,** 2003, "Lower-Troposphere Refractivity Bias in GPS Occultation Retrievals," *J. Geophys. Res.,* 108 (D18), 4577, doi: 10.1029/2002JD003216.

[30] **Xie, F., D. L. Wu, C. O. Ao, E. R. Kursinki, A. J. Mannucci and S. Syndergaard,** 2010, "Super-refraction effects on GPS radio occultation refractivity in marine boundary layers," *Geophys. Res. Lett.,* 37 (L11805), doi: 10.1029/2010GL043299.

[31] **Sun, B., A. Reale, D. J. Seidel and D. C. Hunt,** 2010, "Comparing radiosonde and COSMIC atmospheric profile data to quantify differences among radiosonde types and the effects of imperfect collocation on comparison statistics," *J. Geophys. Res.*, 115 (D23104), 1-16.